

Abstract

Recent studies have shown significant sea surface salinity (SSS) changes at scales ranging from regional to global. In this study, we estimate global salinity means and trends using historical (1950–2014) SSS data from the UK Met. Office Hadley Centre objectively analyzed monthly fields and recent data from the SMOS satellite (2010–2014). We separate the different components (regimes) of the global surface salinity by fitting a Gaussian Mixture Model to the data and using Expectation–Maximization to distinguish the means and trends of the data. The procedure uses a non-subjective method (Bayesian Information Criterion) to extract the optimal number of means and trends. The results show the presence of three separate regimes: Regime A (1950–1990) is characterized by small trend magnitudes; Regime B (1990–2009) exhibited enhanced trends; and Regime C (2009–2014) with significantly larger trend magnitudes. The salinity differences between regime means were around 0.01. The trend acceleration could be related to an enhanced global hydrological cycle or to a change in the sampling methodology.

1 Introduction

Global sea surface salinity (SSS) is changing at scales ranging from regional to global (Antonov et al., 2002; Boyer et al., 2005). Global salinity reflects the balance between surface freshwater flux (evaporation minus precipitation), terrestrial runoff, and mixing and advective processes in the ocean. Thus, changes in salinity are intrinsically connected to alterations in the global hydrological cycle and are expected to be a consequence of climate change (Held and Soden, 2006). The intensification of the global water cycle is expected to be occurring at a rate of $8\% \text{ degree}^{-1}$ of surface warming (Durack et al., 2012) or around 20% considering the projected 2–3° of temperature increase over the next century.

OSD

12, 983–1011, 2015

Changes in surface salinity trend

A. L. Aretxabaleta et al.

Title Page

Abstract

Introduction

Conclusions

References

Tables

Figures

◀

▶

◀

▶

Back

Close

Full Screen / Esc

Printer-friendly Version

Interactive Discussion



Changes in surface salinity trend

A. L. Aretxabaleta et al.

Title Page

Abstract

Introduction

Conclusions

References

Tables

Figures



Back

Close

Full Screen / Esc

Printer-friendly Version

Interactive Discussion



Recently, Antonov et al. (2002) and Boyer et al. (2005) described a general change pattern with surface subtropical areas becoming saltier and high-latitude regions becoming fresher. Curry et al. (2003) found increased salinity in the subtropical evaporation-dominated regions between 25° S and 35° N when they compared the time periods 1955–1969 and 1985–1999 for the entire Atlantic basin. Cravatte et al. (2009) described a large freshening in the Pacific warm pool over the 1955–2003 period.

Hosoda et al. (2009) analyzed global surface salinity comparing Argo float data for the period 2003–2007 with climatological 1960–1989 data from the 2005 World Ocean Database. The recent Argo data showed lower salinities in fresher regions and higher salinities in areas of higher salinity magnitudes. They linked the changes to increased global hydrological cycle during the 30 years between their observations.

Durack and Wijffels (2010) (DW10 herein) analyzed data for the period 1950–2008 and found SSS increases in regions dominated by evaporation while freshening occurred in precipitation-dominated regions. They suggested the change was a consequence of an intensification of the global hydrological cycle. They also provided a comprehensive review of salinity changes in the literature. Using a linear fit for the 1950–2008 data, DW10 found that in a 50 year period, the subtropical gyres (evaporation dominated) exhibited net salinity increases from 0.20 in the eastern south pacific to 0.45 in the subtropical north Atlantic. During the same period, the salinity decreased in the precipitation-dominated regions (for instance, under the Intertropical Convergence Zone, ITCZ), with decreases ranging from –0.25 in the Equatorial Atlantic to –0.57 in the western Equatorial Pacific.

The SSS spatial pattern has been associated with the “rich get richer” mechanism for evaporation-precipitation (Chou et al., 2009). In fact, the enhancement in hydrological cycle has been studied based on the changes in ocean salinity (Schmitt, 2008; Helm et al., 2010; Durack et al., 2012; Durack, 2015). The intensification of the water cycle was larger over 1979–2010 than in earlier periods (1950–1978) related to the accelerated broad-scale warming (Skirris et al., 2014).

Changes in surface salinity trend

A. L. Aretxabaleta et al.

Title Page

Abstract

Introduction

Conclusions

References

Tables

Figures



Back

Close

Full Screen / Esc

Printer-friendly Version

Interactive Discussion



The determination of a single SSS trend by DW10 highlighted significant challenges (e.g., data deficiencies in some regions and times), but it represented only a first step toward a characterization of the time evolution of global salinity. The results of recent analyses of other ocean parameters, such as water level (Church and White, 2006; Ezer, 2013), have demonstrated that changes in the ocean have been accelerated in recent times. In some regions, the rate of change of the water level time series exceeds even a quadratic fit over at least the last 50 years (Church and White, 2006). In fact, the role of salinity on water level changes has also been recently explored (Durack et al., 2014).

The question we are trying to address in this study is whether the SSS changes are due to: (1) a regime shift in which the SSS has moved from one equilibrium state to another (maybe even several regime shifts), (2) a constant SSS trend (no new equilibrium has been achieved), (3) a varying SSS trend (not only is SSS changing, but the rate of change varies); or (4) a combination of the above.

In this study, we separate the different regimes (components with substantially different characteristics) of the global SSS (1950–2014) by fitting Gaussian Mixture Models (GMM) with and without trends to the SSS data to characterize, not only the means, but also the trends. The GMMs are estimated using an Expectation–Maximization algorithm with the number of components determined non-subjectively by the Bayesian Information Criterion to extract the optimal number of means and trends. The long-term global SSS dataset from the UK Met. Office Hadley Centre (Good et al., 2013) is chosen as the reference data source. Recently available SMOS satellite data is used as a complement for the period 2010–2014.

2 Data and methods

2.1 Long-term global salinity data

The Met Office Hadley Centre provides global quality controlled ocean temperature and salinity profiles and monthly long-term objectively analyzed global fields with a one degree spatial resolution (Ingleby and Huddleston, 2007; Good et al., 2013). The most recent EN4 dataset includes objectively analyzed fields formed from profile data with uncertainty estimates. The available data extend from 1900 to the present and there are separate files for each month. Good et al. (2013) used a simple Analysis Correction (Lorenc et al., 1991) optimal interpolation methodology to analyze global historical observations that had been methodically quality controlled. The analysis fields were constructed by combining a background field (the analysis field of the previous month) with the quality controlled profiles from the month being analyzed.

In this work, the surface salinity field (top layer of the dataset) from 1950 to 2014 is used. The 1950 cutoff was chosen to match previous trend studies (Boyer et al., 2005; Durack and Wijffels, 2010) and to prevent data-deficient periods.

2.2 SMOS satellite data

The recently available SMOS (Soil Moisture and Ocean Salinity) satellite (Font et al., 2010, 2012) provides sea surface salinity data with sufficient spatial resolution ($1/4^\circ$) to characterize global (Xie et al., 2014) and regional (e.g., Amazon: Aretxabaleta and Smith, 2013; North Atlantic SSS maximum: Hernandez et al., 2014; Kolodziejczyk et al., 2015; Gulf Stream: Reul et al., 2014; northern North Atlantic: Köhler et al., 2015) features. Recently, SMOS data have been used to study salinity variability in the Atlantic (Tzortzi et al., 2013), the signature of La Niña in the tropical Pacific Ocean (Hasson et al., 2014) and even create surface T/S diagrams (Sabia et al., 2014). Level 3 (global maps) data were obtained from the CP34 distribution center at the SMOS Barcelona Expert Centre (<http://tarod.cmima.csic.es>) for the period 2010–2014. The

Changes in surface salinity trend

A. L. Aretxabaleta et al.

Title Page

Abstract

Introduction

Conclusions

References

Tables

Figures



Back

Close

Full Screen / Esc

Printer-friendly Version

Interactive Discussion



temporal resolution of the objectively analyzed SMOS data is one month and the spatial resolution is $1/4^\circ$. We averaged the data to one degree resolution to match the long-term dataset and reduce noisy signals.

The SMOS satellite data exhibited deficiencies near coastal areas and in high latitudes (Guimbard et al., 2012; Yin et al., 2014; Hernandez et al., 2014; Köhler et al., 2015). To prevent the introduction of bogus features, those data were removed from the analysis. The main areas affected were in high latitudes, in the proximity of continents, the Mediterranean, and in a large area of the western Pacific surrounding the Philippines and Japan.

2.3 Gaussian mixture models and expectation-maximization

A Gaussian Mixture Model (GMM) is a probabilistic model for which the probability density function is a combination of two or more Gaussian distributions. The Expectation–Maximization (EM) algorithm is an iterative procedure to find a Maximum Likelihood Estimate (MLE) of the parameters of a GMM. In the past, the EM algorithm was used to separate the regimes of a spatial time series (Smith and Aretxabaleta, 2007) and to find the best GMM describing the joint distribution of model and data in a model skill assessment scenario (Aretxabaleta and Smith, 2011). In previous studies, EM was used to estimate missing values for oceanographic datasets (Houseago-Stokes and Challenor, 2004; Kondrashov and Ghil, 2006). Aretxabaleta and Smith (2013) introduced a measurement operator (H) and error (assuming the observations were unbiased with a Gaussian measurement error $\epsilon(t) \sim G(0, R(t))$ of known covariance, $R(t)$), to provide a more general algorithm that could be used for missing data and interpolation problems.

In this implementation, we introduce the possibility of defining the GMM by both a mean and a linear temporal trend. After we have found the number of components (representing probability density functions), n_c , component distributions (mean, trend, and covariance), $G(\mu^k, \alpha^k, \Sigma^k)$, and their respective likelihoods, τ^k , we can conduct an Empirical Orthogonal Function (EOF) analysis on the Σ^k .

Changes in surface salinity trend

A. L. Aretxabaleta et al.

Title Page

Abstract

Introduction

Conclusions

References

Tables

Figures



Back

Close

Full Screen / Esc

Printer-friendly Version

Interactive Discussion



the k th component distribution, $n^k = \sum_t w^k(t)$, is computed and normalized,

$$\tau^k = \frac{n^k}{n_t} = \frac{\sum_t w^k(t)}{n_t}, \quad (4)$$

where n_t is the length of the time series.

We enforced that the time series is an autoregressive process of order one (AR(1)) to avoid rapid switching between regimes. Thus, the salinity at time t depends linearly on the previous value, $d(t) = c + \varphi d(t-1) + \varepsilon_t$, where c is a constant, φ is the parameter of the AR(1) model and ε_t is white noise.

An EOF analysis can be conducted based on the component distributions covariances, Σ^k . Using the eigenvectors of Σ^k , we obtain a new set of orthogonal basis functions that are meaningful for times when $w^k(t) \simeq 1$. The EOF analysis can be considered independently during different regimes in a similar approach to Tipping and Bishop (1999).

Our approach is related to the multivariate adaptive regression splines (MARS) method (Friedman, 1991) as both automatically determine the number and timing of the separation between regimes (breakpoints or knots) based on the data. The main difference between the two approaches is that our method includes multiple spatial location (multiple time series) and the regime extraction is across the complete dataset.

2.4 Non-subjective choice of number of regimes: Bayesian Information Criterion

To determine the optimal number of components (regimes) in the GMM, we use the Bayesian Information Criterion (BIC, Schwarz, 1978; Aretxabaleta and Smith, 2011). The BIC is an empirical approach that approximates the total probability (Bayes factor) of a probability distribution under some set data,

$$\text{BIC}(k) = -2 \log(\hat{p}(\psi | \mu^1, \dots, \mu^{n_c}, \alpha^1, \dots, \alpha^{n_c}, \Sigma^1, \dots, \Sigma^{n_c}, \tau^1, \dots, \tau^{n_c})) - D_k \log(n_t). \quad (5)$$

The penalty term preventing over-fitting, D_k , for a GMM with n_c components and n time series is $D_k = n_c n(n+2)/2 + n_c - 1$, where $n_c n$ of those are for the means of each distribution, another $n_c n$ correspond to the trends, $n_c n(n-1)/2$ are for the parameters of the covariance matrix, and $n_c - 1$ for the τ_k .

There are a number of potential combinations of means and trends (Fig. 1) that can be fitted to any spatial time series. In the current application, the Expectation–Maximization (EM) algorithm is used to find the best GMM describing the data distribution. The method is run under several possible scenarios that separate regimes based on including only means, means and a global trend, and a combination of means and trends. The BIC approach penalizes excessive number of parameters with D_k being adjusted depending on the inclusion/exclusion of trends. BIC is used twice in the current procedure: first, to choose the optimal number of components in a particular scenario (e.g., only means, combining means and trends), and second, to choose among the different scenarios.

3 Results

3.1 Comparison with DW10

The Hadley Centre EN4 surface salinity interpolated fields incorporated quality controlled observations in a similar manner as the database used by Durack and Wijffels (2010) to create the DW10 surface fields. DW10 fields were reported for a 50 year period (nominally 1950–2000) to simplify comparisons, even though they used data from 1950 to 2008. To establish whether the datasets were sufficiently similar, we calculated the mean and trend for the same period as DW10 (1950–2008) using the interpolated data (Fig. 2). The climatological mean surface salinity (Fig. 2a) exhibits the same general structure and magnitude as the DW10 results. The standard deviation of the surface salinity (Fig. 2b) highlights the increased variability associated with river discharge, the ITCZ, and intense meandering current systems like the Gulf Stream. As in

Changes in surface salinity trend

A. L. Aretxabaleta et al.

Title Page

Abstract

Introduction

Conclusions

References

Tables

Figures



Back

Close

Full Screen / Esc

Printer-friendly Version

Interactive Discussion



Changes in surface salinity trend

A. L. Aretxabaleta et al.

Title Page

Abstract

Introduction

Conclusions

References

Tables

Figures



Back

Close

Full Screen / Esc

Printer-friendly Version

Interactive Discussion



the case of the mean, the 50 year linear surface salinity trend (Fig. 2c) is also similar to the published fields with minimal differences. For instance, there is a slightly less negative trend in the Equatorial and North Atlantic and a larger positive trend in the Antarctic Circumpolar Current region in our results. Overall, the trend magnitude and spatial distribution for the 1950–2008 period are equivalent in both datasets. The main trend features include a predominantly positive trend in the Atlantic, southeastern Pacific, and Indian Ocean, and a predominantly negative trend in the north and western Pacific and along the Antarctic Circumpolar Current region.

3.2 Regime separation using Hadley Centre EN4 1950–2014 fields

When the global SSS monthly data from the Hadley Centre EN4 were analyzed, the EM method distinguished three separate regimes. These regimes are characterized by different means but also different trends (Figs. 3 and 4). The separation (break-point) between the first two regimes (Regime A and B) occurs in May 1990, while the separation between the second and third regimes (Regime B and C) was found to be March 2009.

The global surface salinity means for the three regimes (Fig. 3) exhibited the same general pattern with higher salinity in the subtropical gyres and lower values in the sub-polar, polar regions, and under the ITCZ. The differences between regime means were on the order of 0.1 (0.099 rms difference between Regime A and B; and 0.15 between Regime B and C). The Regime B (1990–2009) average was saltier than Regime A (1950–1990) in most of the Atlantic Ocean except along the eastern US, in the central equatorial region, and south of 30° S. In contrast most of the Pacific (except for the southwest) was fresher in Regime B than A. The difference between the average salinities of Regime B (1990–2009) and Regime C (2009–2014) exhibited saltier values in the later period in most of the Pacific and South Atlantic, while a large part of the North Atlantic was fresher during Regime C.

The trend for Regime A (1950–1990, Fig. 4a) was consistent with the results obtained by DW10 (Durack and Wijffels (2010) and Fig. 2, note the different scale) and

Changes in surface salinity trend

A. L. Aretxabaleta et al.

Title Page

Abstract

Introduction

Conclusions

References

Tables

Figures



Back

Close

Full Screen / Esc

Printer-friendly Version

Interactive Discussion



the references therein. The differences were a slightly larger positive trend in the Equatorial Atlantic and a lack of positive trend in the eastern Pacific. The trend for Regime B (1990–2009, Fig. 4b) exhibited larger positive magnitudes in the North and South Atlantic than Regime A, a negative trend ($\sim -0.02 \text{ yr}^{-1}$) along the Equatorial Atlantic, negative trends in the areas of the Antarctic Circumpolar Current and positive trends ($0.01\text{--}0.02 \text{ yr}^{-1}$) in most of the Pacific between 30° S and 30° N . The trend associated with Regime B exhibited enhanced magnitudes when compared to Regime A (positive trends were more positive and negative areas were more negative during Regime B). In both regimes the trends are consistent with an intensification of the global hydrological cycle (Schanze et al., 2010; Yu, 2011). The estimated trend during Regime C (2009–2014, Fig. 4c) was much larger than in any of the two early regimes. The Regime C trend was negative in the majority of the North Atlantic (up to -0.04 yr^{-1}), eastern Indian Ocean ($\sim -0.05 \text{ yr}^{-1}$) and western ($< -0.05 \text{ yr}^{-1}$) and south equatorial ($\sim -0.03 \text{ yr}^{-1}$) Pacific. Positive trends during Regime C were estimated along the western part of the Equatorial and South Atlantic (up to 0.06 yr^{-1}), the Pacific subtropical gyres (ranging $0.02\text{--}0.05 \text{ yr}^{-1}$) and the western Indian Ocean ($\sim 0.04 \text{ yr}^{-1}$).

The salinity time evolution showed the changing temporal pattern during the full record and the potential distinction between regimes (Fig. 5). For instance, the Equatorial Atlantic (Fig. 5a, $5^\circ \text{ S}\text{--}5^\circ \text{ N}$) showed a notable difference between the trends for the three regimes, while the difference between the average salinity of the three regimes was small. The North Atlantic Subtropical Gyre (Fig. 5b, $15\text{--}30^\circ \text{ N}$) in contrast exhibited noticeable differences in the trends, but especially in the means between the three regimes. Meanwhile, the most striking feature in the Mediterranean (Fig. 5c) and in the Equatorial Pacific (Fig. 5d, $5^\circ \text{ S}\text{--}5^\circ \text{ N}$) was the sharp drop in salinity associated with El Niño events while the main difference between regimes was again in the magnitude of the trend. The largest trend acceleration between regimes was present in the Mediterranean (Fig. 5c).

As described in Sect. 2.3, the EM algorithm also allowed for the separation of the modes of variability. The 1st EOF for Regime A and B explained over 75 % of the vari-

Changes in surface salinity trend

A. L. Aretxabaleta et al.

Title Page

Abstract

Introduction

Conclusions

References

Tables

Figures



Back

Close

Full Screen / Esc

Printer-friendly Version

Interactive Discussion



ance (79 and 77 %, respectively) while only explaining 67 % of the Regime C variance. Meanwhile, the 2nd EOF explained 11, 12 and 14 % of the variance in each regime. The 1st EOF of Regime A was spatially consistent with Regime B, but its magnitude was smaller (Fig. 6). The 1st EOF in the first two regimes suggested the Atlantic and southeastern Pacific were fluctuating in phase, while the western Pacific and most of the Southern Ocean were out of phase. The 1st EOF of Regime C exhibited a different spatial pattern and larger magnitude with the separation between basins being less apparent, with the main feature likely associated with the northern/southern migration and extent of the ITCZ. The 2nd EOF for the first two regimes was quite similar with positive values in most areas except the Antarctic and Equatorial Pacific oceans. Meanwhile, the 2nd EOF of Regime C was mostly consistent with the Pacific and Atlantic oceans being out of phase. The time series of the 1st EOF (Fig. 7a) showed larger short-term fluctuations for Regime B and Regime C, with Regime B exhibiting a trend in time. There was an apparent relationship between the 2nd EOF for Regime B (Fig. 7b) and the ENSO cycle (1998, 2003, 2005 peaks), while no clear relation appeared to be present for Regime A or C.

3.3 Regime separation with updated SMOS fields 2010–2014

The recent availability of global surface salinity fields from satellites (SMOS and Aquarius) provided the possibility of using alternative data that were not included as part of the Good et al. (2013) dataset. The goal was to analyze the robustness of the regime separation by replacing the recent (2010–2014) fields with satellite-derived products.

The inclusion of the available 5 years of SMOS data in the analysis in substitution of the EN4 data for 2010–2014 slightly altered the EM separation results (Figs. 8 and 9). The EM method also distinguished three separate regimes (A', B', and C') with different means and trends. The breakpoint between Regime A' and B' was in July 1988 and between Regime B' and C' in January 2010. The difference in the separation (breakpoint) dates between the early regimes was expected as the merged dataset did not include

several areas (proximity to coastal areas, Mediterranean Sea, high latitude) that were present in the original EN4 dataset.

The means and differences of the two first regimes (Fig. 8a, b and d) were equivalent to the results for the complete EN4 dataset (Fig. 3). The average salinity for Regime C' (Fig. 8c) exhibited significant differences from both the Regime B' mean and also from the third regime of the original dataset (Regime C, 2009–2014). The mean salinity during Regime C' was fresher in the North (up to -0.5) and Equatorial Atlantic, the Indian and western Pacific Oceans, while being saltier in most of the Southern Ocean and in large areas of the Pacific Ocean.

As was the case with the means, the trends of the two first regimes (A' and B') of the combined time series (Fig. 9a, b) were equivalent to the trends extracted from the original dataset (Fig. 4) for Regimes A and B. The trend for Regime C' (2010–2014, Fig. 9c) differed in magnitude and spatial structure from the trend for Regime C of the original EN4 dataset (2009–2014, Fig. 4c). The Regime C' trend was positive in the Equatorial Pacific and Atlantic while having a negative trend in most of the rest of the oceans with large negative values especially in the North Atlantic. The trend for Regime C' was likely the effect of changes in the processing methodology for global SMOS data (Guimbard et al., 2012; Yin et al., 2014).

4 Discussion

While the study focuses on the near-surface salinity, the vertical extent of the changes can be much larger. Boyer et al. (2005) described significant changes with varying vertical range depending on the basin (500 m in the Pacific, 1000 m in the Indian, and 3000 m in the Atlantic Ocean). The vertical extent of the increased salinity seems to be larger than the extent in areas of freshening. The relationship between salinity and density complicates the basic hypothesis of salinity changes being primarily surface forced (Durack and Wijffels, 2010; Durack, 2015). The combined temperature and salinity

Changes in surface salinity trend

A. L. Aretxabaleta et al.

Title Page

Abstract

Introduction

Conclusions

References

Tables

Figures



Back

Close

Full Screen / Esc

Printer-friendly Version

Interactive Discussion



changes need to be understood to explain the observed changes, especially in the interior of the water column.

The described salinity change acceleration is likely the result of global hydrological cycle intensification as was suggested by Hosoda et al. (2009) and Durack and Wijffels (2010). The areas of enhanced precipitation and evaporation (Schanze et al., 2010; Yu, 2011) correspond with the largest magnitude changes in salinity (Chou et al., 2009). The changing trend in salinity will enhance even farther the hydrological cycle intensification described in Durack et al. (2012) with modifications larger than the proposed 20% in the next century.

While our most recent period (2009–2014) might be too short to be considered a robust regime change, the differences in mean and trend between the two early regimes (A: 1950–1990; and B: 1990–2009) are consistent with the idea of salinity change acceleration caused by enhanced hydrological cycle. The water cycle has been shown to be farther increased in the period 1979–2010 due to accelerated warming (Skiriris et al., 2014). Durack et al. (2012) analyzed modeling scenarios for the 20th century (Coupled Model Intercomparison Project Phase 3, CMIP3, Meehl et al., 2007) that are consistent with not only a linear increase in hydrological cycle magnitude but also an acceleration of the intensification. The CMIP3 scenarios showed the expected intensification of existing patterns of global mean E-P (“rich get richer” mechanism) and the resulting salinity pattern amplification. The changes calculated from ocean observations were consistent with the scenario simulations but with a slightly larger effect of global surface warming on salinity pattern amplification (Durack et al., 2012). The spatial patterns in the CMIP3 climate simulations matched the observed salinity pattern in many areas and were consistent with the spatial structure in the present study.

As the sampling methodology and number of observations have evolved in time, the trend acceleration in recent times might not be a completely realistic feature. Skiriris et al. (2014) suggested that while water cycle intensification was consistent with the warming trend, it also matched the improved salinity sampling. The availability of extensive field cruises in the last few decades and especially the development of the Argo

Changes in surface salinity trend

A. L. Aretxabaleta et al.

Title Page

Abstract

Introduction

Conclusions

References

Tables

Figures



Back

Close

Full Screen / Esc

Printer-friendly Version

Interactive Discussion



Changes in surface salinity trend

A. L. Aretxabaleta et al.

Title Page

Abstract

Introduction

Conclusions

References

Tables

Figures



Back

Close

Full Screen / Esc

Printer-friendly Version

Interactive Discussion



network of profiling drifters over the last 15 years have altered the quantity, quality and spatial coverage of observations. The Argo network was established in 2001 and since 2006 has maintained more than 3000 active floats resulting in a nominal horizontal sampling of around 300 km. The result is a more intense sampling of the global salinity in recent years and also a switch from cruise-dependent locally intense sampling to more automatic sampling by profilers, floats and gliders. The changing trends can be the result of the changing measurement methodologies and spatial and temporal resolutions. Proper quality control of recent measurements will minimize this effect.

High quality global surface salinity fields that consider multiple instrument sources, measurement error and instrument quality are currently being developed (Hoareau et al., 2014; Xie et al., 2014). Careful validation of any new data is fundamental for the success of the EM method or any other procedure to characterize the means and trends of long-term datasets.

5 Summary and conclusions

In this study, we have analyzed global salinity datasets to identify a series of regimes characterized by fluctuations around a changing average and temporal tendency (trend). The separation between regimes is achieved through the analysis of global features fitting a Gaussian Mixture Model to the data and using an Expectation–Maximization algorithm to determine the parameters that best describe the spatial salinity time series. The datasets used include global monthly fields from 1950 to 2014 with a global resolution of one degree.

The EM method allows for the separation of regimes based on their averages and trends assuming the spatial time series is a combination of Gaussians (GMM). The method uses Bayesian Information Criterion to choose the appropriate number of means/trends by penalizing excessive overfitting. The resulting fit represents the Maximum Likelihood Estimate (MLE) chosen using a non-arbitrary separation.

Changes in surface salinity trend

A. L. Aretxabaleta et al.

Title Page

Abstract

Introduction

Conclusions

References

Tables

Figures



Back

Close

Full Screen / Esc

Printer-friendly Version

Interactive Discussion



The method distinguished between three regimes characterized by distinct mean and trend. Regime A (1950–1990) was similar to the long-term average and trend described in several recent studies (Boyer et al., 2005; Cravatte et al., 2009; Durack and Wijffels, 2010). Regime B (1990–2009) was characterized by a similar average with slightly fresher Pacific and saltier Atlantic but with larger trend magnitudes that are consistent with an enhanced global hydrological cycle. Regime C (2009–2014) showed a further intensification of the trend magnitudes with generally more positive trends in large areas of the Southern Hemisphere and negative trends in the North Atlantic, eastern Indian and western Pacific oceans. When the last 5 years of data (2010–2014) were replaced by salinity measured by the SMOS satellite, the separation between regimes, while not completely equal, exhibited similar spatial and temporal features demonstrating the robustness of the method.

A future goal is to use satellite data from SMOS and Aquarius to determine if the estimated means and trends are realistic. The combination of densely distributed in-situ observations (Argo profilers) and remotely sensed satellite data will provide a better approximation to the evolving global salinity field.

Acknowledgements. The historical time series was obtained from the UK Met Office Hadley Centre (<http://www.metoffice.gov.uk/hadobs/en4/>). The SMOS data were produced by the Barcelona Expert Centre (www.smos-bec.icm.csic.es), a joint initiative of the Spanish Research Council (CSIC) and the Technical University of Catalonia (UPC), mainly funded by the Spanish National Program on Space. The authors thank the efforts of the entire SMOS-BEC to produce improved SSS products while being an outstanding working environment. The authors thank Ray W. Schmitt (WHOI) for his support and comments on the manuscript. A. L. Aretxabaleta was supported by a Juan de la Cierva grant from the Spanish Government during the early stages of the study. K. W. Smith was supported by his wages at Lowe Energy Design.

References

- Antonov, J. I., Levitus, S., and Boyer, T. P.: Steric sea level variations during 1957–1994: importance of salinity, *J. Geophys. Res.*, 107, 8013, doi:10.1029/2001JC000964, 2002. 984, 985
- 5 Aretxabaleta, A. L. and Smith, K. W.: Analyzing state-dependent model-data comparison in multi-regime systems, *Comput. Geosci.*, 15, 627–636, 2011. 988, 990
- Aretxabaleta, A. L. and Smith, K. W.: Multi-regime non-Gaussian data filling for incomplete ocean datasets, *J. Marine Syst.*, 119, 11–18, 2013. 987, 988
- Boyer, T. P., Levitus, S., Antonov, J. I., Locarnini, R. A., and Garcia, H. E.: Linear trends in salinity for the World Ocean, 1955–1998, *Geophys. Res. Lett.*, 32, L01604, doi:10.1029/2004GL021791, 2005. 984, 985, 987, 995, 998
- 10 Chou, C., Neelin, J. D., Chen, C.-A., and Tu, J.-Y.: Evaluating the “rich-get-richer” mechanism in tropical precipitation change under global warming, *J. Climate*, 22, 1982–2005, 2009. 985, 996
- Church, J. A. and White, N. J.: A 20th century acceleration in global sea-level rise, *Geophys. Res. Lett.*, 33, L01602, doi:10.1029/2005GL024826, 2006. 986
- Cravatte, S., Delcroix, T., Zhang, D., McPhaden, M., and Leloup, J.: Observed freshening and warming of the western Pacific warm pool, *Clim. Dynam.*, 33, 565–589, 2009. 985, 998
- Curry, R., Dickson, R. R., and Yashayaev, I.: A change in the fresh-water balance of the Atlantic Ocean over the past four decades, *Nature*, 426, 826–829, 2003. 985
- 20 Durack, P. J.: Ocean salinity and the global water cycle, *Oceanography*, 28, 20–31, doi:10.5670/oceanog.2015.03, 2015. 985, 995
- Durack, P. J. and Wijffels, S. E.: Fifty-year trends in global ocean salinities and their relationship to broad-scale warming, *J. Climate*, 23, 4342–4362, 2010. 985, 987, 991, 992, 995, 996, 998, 1004
- 25 Durack, P. J., Wijffels, S. E., and Matear, R. J.: Ocean salinities reveal strong global water cycle intensification during 1950 to 2000, *Science*, 336, 455–458, 2012. 984, 985, 996
- Durack, P. J., Wijffels, S. E., and Gleckler, P. J.: Long-term sea-level change revisited: the role of salinity, *Environ. Res. Lett.*, 9, 114017, doi:10.1088/1748-9326/9/11/114017, 2014. 986
- 30 Ezer, T.: Sea level rise, spatially uneven and temporally unsteady: why the US east coast, the global tide gauge record, and the global altimeter data show different trends, *Geophys. Res. Lett.*, 40, 5439–5444, 2013. 986

Changes in surface salinity trend

A. L. Aretxabaleta et al.

Title Page

Abstract

Introduction

Conclusions

References

Tables

Figures



Back

Close

Full Screen / Esc

Printer-friendly Version

Interactive Discussion



Changes in surface salinity trend

A. L. Aretxabaleta et al.

Title Page

Abstract

Introduction

Conclusions

References

Tables

Figures



Back

Close

Full Screen / Esc

Printer-friendly Version

Interactive Discussion



Font, J., Camps, A., Borges, A., Martín-Neira, M., Boutin, J., Reul, N., Kerr, Y., Hahne, A., and Mecklenburg, S.: SMOS: the challenging sea surface salinity measurement from space, *Proceedings of the IEEEv*, 98, 649–665, 2010. 987

Font, J., Ballabrera-Poy, J., Camps, A., Corbella, I., Duffo, N., Duran, I., Emelianov, M., Enrique, L., Fernández, P., Gabarró, C., Gonzalez, C., Gonzalez, V., Gourrion, J., Guimbard, S., Hoareau, N., Julia, A., Kalaroni, S., Konstantinidou, A., Aretxabaleta, A. L., Martinez, J., Miranda, J., Monerris, A., Montero, S., Murre, B., Perez, M. P. F., Piles, M., Portabella, M., Sabia, R., Salvador, J., Talone, M., Torres, F., Turiel, A., Vall-Llossera, M., and Villarino, R.: A new space technology for ocean observation: the SMOS mission, *Sci. Mar.*, 76, 249–259, 2012. 987

Friedman, J. H.: Multivariate adaptive regression splines, *Ann. Stat.*, 1, 1–67, doi:10.1214/aos/1176347963, 1991. 990

Good, S. A., Martin, M. J., and Rayner, N. A.: EN4: quality controlled ocean temperature and salinity profiles and monthly objective analyses with uncertainty estimates, *J. Geophys. Res.-Oceans*, 118, 6704–6716, 2013. 986, 987, 994

Guimbard, S., Gourrion, J., Portabella, M., Turiel, A., Gabarro, C., and Font, J.: SMOS semi-empirical ocean forward model adjustment, *IEEE T. Geosci. Remote*, 50, 1676–1687, 2012. 988, 995

Hasson, A., Delcroix, T., Boutin, J., Dussin, R., and Ballabrera-Poy, J.: Analyzing the 2010–2011 La Niña signature in the tropical Pacific sea surface salinity using in situ data, SMOS observations, and a numerical simulation, *J. Geophys. Res.*, 119, 3855–3867, doi:10.1002/2013JC009388, 2014. 987

Held, I. M. and Soden, B. J.: Robust responses of the hydrological cycle to global warming, *J. Climate*, 19, 5686–5699, 2006. 984

Helm, K. P., Bindoff, N. L., and Church, J. A.: Changes in the global hydrological-cycle inferred from ocean salinity, *Geophys. Res. Lett.*, 37, L18701, doi:10.1029/2010GL044222, 2010. 985

Hernandez, O., Boutin, J., Kolodziejczyk, N., Reverdin, G., Martin, N., Gaillard, F., Reul, N., and Vergely, J.: SMOS salinity in the subtropical north Atlantic salinity maximum: 1. Comparison with Aquarius and in situ salinity, *J. Geophys. Res.*, 119, 8878–8896, doi:10.1002/2013JC009610, 2014. 987, 988

Changes in surface salinity trend

A. L. Aretxabaleta et al.

Title Page

Abstract

Introduction

Conclusions

References

Tables

Figures



Back

Close

Full Screen / Esc

Printer-friendly Version

Interactive Discussion



- Hoareau, N., Umbert, M., Martínez, J., Turiel, A., and Ballabrera-Poy, J.: On the potential of data assimilation to generate SMOS-Level 4 maps of sea surface salinity, *Remote Sens. Environ.*, 146, 188–200, 2014. 997
- Hosoda, S., Sugo, T., Shikama, N., and Mizuno, K.: Global surface layer salinity change detected by Argo and its implication for hydrological cycle intensification, *J. Oceanogr.*, 65, 579–586, 2009. 985, 996
- Houseago-Stokes, R. E. and Challenor, P. G.: Using PPCA to estimate EOFs in the presence of missing values, *J. Atmos. Ocean. Tech.*, 21, 1471–1480, 2004. 988
- Ingleby, B. and Huddleston, M.: Quality control of ocean temperature and salinity profiles – historical and real-time data, *J. Marine Syst.*, 65, 158–175, 2007. 987
- Köhler, J., Sena Martins, M., Serra, N., and Stammer, D.: Quality assessment of spaceborne sea surface salinity observations over the northern North Atlantic, *J. Geophys. Res.-Oceans*, 120, 94–112, doi:10.1002/2014JC010067, 2015. 987, 988
- Kolodziejczyk, N., Hernandez, O., Boutin, J., and Reverdin, G.: SMOS salinity in the subtropical North Atlantic salinity maximum: 2. Two-dimensional horizontal thermohaline variability, *J. Geophys. Res.-Oceans*, 120, 972–987, doi:10.1002/2014JC010103, 2015. 987
- Kondrashov, D. and Ghil, M.: Spatio-temporal filling of missing points in geophysical data sets, *Nonlin. Processes Geophys.*, 13, 151–159, doi:10.5194/npg-13-151-2006, 2006. 988
- Lorenc, A., Bell, R., and Macpherson, B.: The Meteorological Office analysis correction data assimilation scheme, *Q. J. Roy. Meteor. Soc.*, 117, 59–89, 1991. 987
- Meehl, G. A., Covey, C., Taylor, K. E., Delworth, T., Stouffer, R. J., Latif, M., McAvaney, B., and Mitchell, J. F.: The WCRP CMIP3 multimodel dataset: a new era in climate change research, *B. Am. Meteorol. Soc.*, 88, 1383–1394, 2007. 996
- Reul, N., Chapron, B., Lee, T., Donlon, C., Boutin, J., and Alory, G.: Sea surface salinity structure of the meandering Gulf Stream revealed by SMOS sensor, *Geophys. Res. Lett.*, 41, 3141–3148, doi:10.1002/2014GL059215, 2014. 987
- Sabia, R., Klockmann, M., Fernandez-Prieto, D., and Donlon, C.: A first estimation of SMOS-based ocean surface T-S diagrams, *J. Geophys. Res.-Oceans*, 119, 7357–7371, doi:10.1002/2014JC010120, 2014. 987
- Schanze, J. J., Schmitt, R. W., and Yu, L.: The global oceanic freshwater cycle: a state-of-the-art quantification, *J. Mar. Res.*, 68, 569–595, 2010. 993, 996
- Schmitt, R. W.: Salinity and the global water cycle, *Oceanography*, 21, 12–19, 2008. 985
- Schwarz, G.: Estimating the dimension of a model, *Ann. Stat.*, 6, 461–464, 1978. 990

- Skliris, N., Marsh, R., Josey, S. A., Good, S. A., Liu, C., and Allan, R. P.: Salinity changes in the World Ocean since 1950 in relation to changing surface freshwater fluxes, *Clim. Dynam.*, 43, 709–736, 2014. 985, 996
- Smith, K. W. and Aretxabaleta, A. L.: Expectation–Maximization analysis of spatial time series, *Nonlin. Processes Geophys.*, 14, 73–77, doi:10.5194/npg-14-73-2007, 2007. 988
- 5 Tipping, M. E. and Bishop, C. M.: Probabilistic principal component analysis, *J. Roy. Stat. Soc. B*, 61, 611–622, 1999. 990
- Tzortzi, E., Josey, S. A., Srokosz, M., and Gommenginger, C.: Tropical Atlantic salinity variability: new insights from SMOS, *Geophys. Res. Lett.*, 40, 2143–2147, doi:10.1002/grl.50225, 10 2013. 987
- Xie, P., Boyer, T., Bayler, E., Xue, Y., Byrne, D., Reagan, J., Locarnini, R., Sun, F., Joyce, R., and Kumar, A.: An in situ-satellite blended analysis of global sea surface salinity, *J. Geophys. Res.-Oceans*, 119, 6140–6160, 2014. 987, 997
- Yin, X., Boutin, J., Martin, N., Spurgeon, P., Vergely, J.-L., and Gaillard, F.: Errors in SMOS sea surface salinity and their dependency on a priori wind speed, *Remote Sens. Environ.*, 146, 159–171, 2014. 988, 995
- 15 Yu, L.: A global relationship between the ocean water cycle and near-surface salinity, *J. Geophys. Res.*, 116, C10025, doi:10.1029/2010JC006937, 2011. 993, 996

Changes in surface salinity trend

A. L. Aretxabaleta et al.

[Title Page](#)[Abstract](#)[Introduction](#)[Conclusions](#)[References](#)[Tables](#)[Figures](#)[◀](#)[▶](#)[◀](#)[▶](#)[Back](#)[Close](#)[Full Screen / Esc](#)[Printer-friendly Version](#)[Interactive Discussion](#)

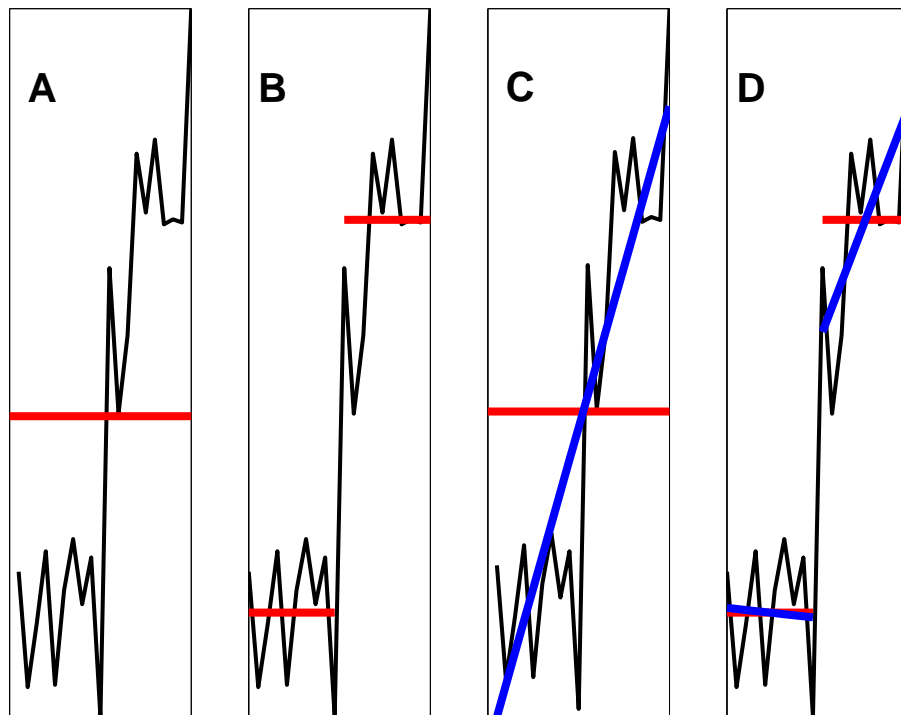


Figure 1. Schematic of fit to an idealized time series (black) with varying number of parameters (means in red, trends in blue): **(a)** one mean, **(b)** two means, **(c)** one mean and one trend; and **(d)** two means and two trends.

Changes in surface salinity trend

A. L. Aretxabaleta et al.

Title Page	
Abstract	Introduction
Conclusions	References
Tables	Figures
◀	▶
◀	▶
Back	Close
Full Screen / Esc	
Printer-friendly Version	
Interactive Discussion	



Changes in surface salinity trend

A. L. Aretxabaleta et al.

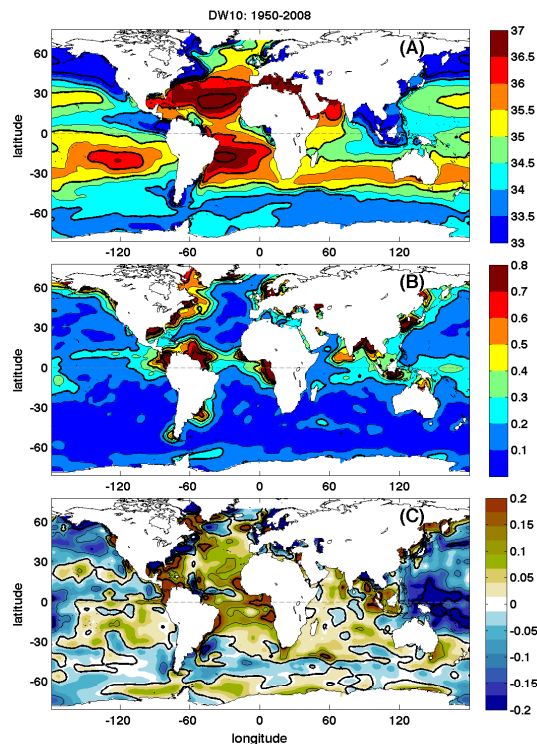


Figure 2. Mean and trend for the 1950–2008 period using EN4 data equivalent to Fig. 5 of Durack and Wijffels (2010). **(a)** 1950–2008 climatological mean surface salinity. Contours of salinity every 0.5 are plotted in black with thicker contours every 1. **(b)** 1950–2008 climatological standard deviation of surface salinity. Contours of standard deviation every 0.1 are plotted in black with thicker contours every 0.2. **(c)** 50 year linear surface salinity trend [$\text{pss} (50 \text{ yr})^{-1}$]. Contours every 0.2 are plotted in black.

Title Page

Abstract

Introduction

Conclusions

References

Tables

Figures



Back

Close

Full Screen / Esc

Printer-friendly Version

Interactive Discussion



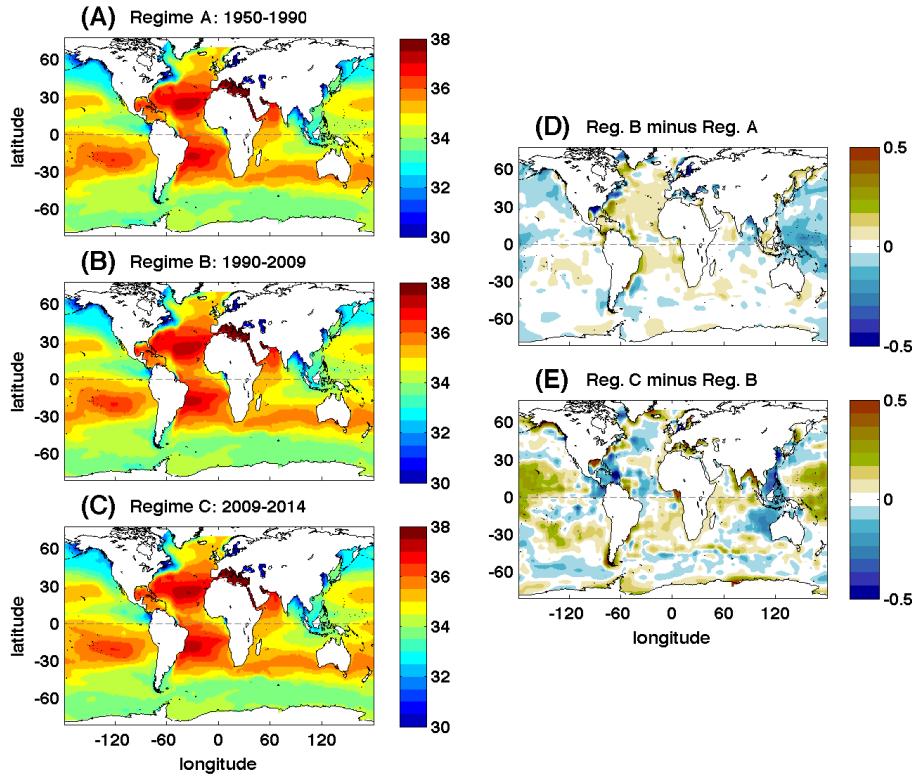


Figure 3. Mean surface salinity for the three regimes estimated by the EM procedure using EN4 1950–2014 data: **(a)** Regime A: 1950–1990, **(b)** Regime B: 1990–2009; and **(c)** Regime C: 2009–2014. The right panels include the differences between the means of **(d)** Regime B and A; and **(e)** Regime C and B.

Changes in surface salinity trend

A. L. Aretxabaleta et al.

Title Page	
Abstract	Introduction
Conclusions	References
Tables	Figures
◀	▶
◀	▶
Back	Close
Full Screen / Esc	
Printer-friendly Version	
Interactive Discussion	



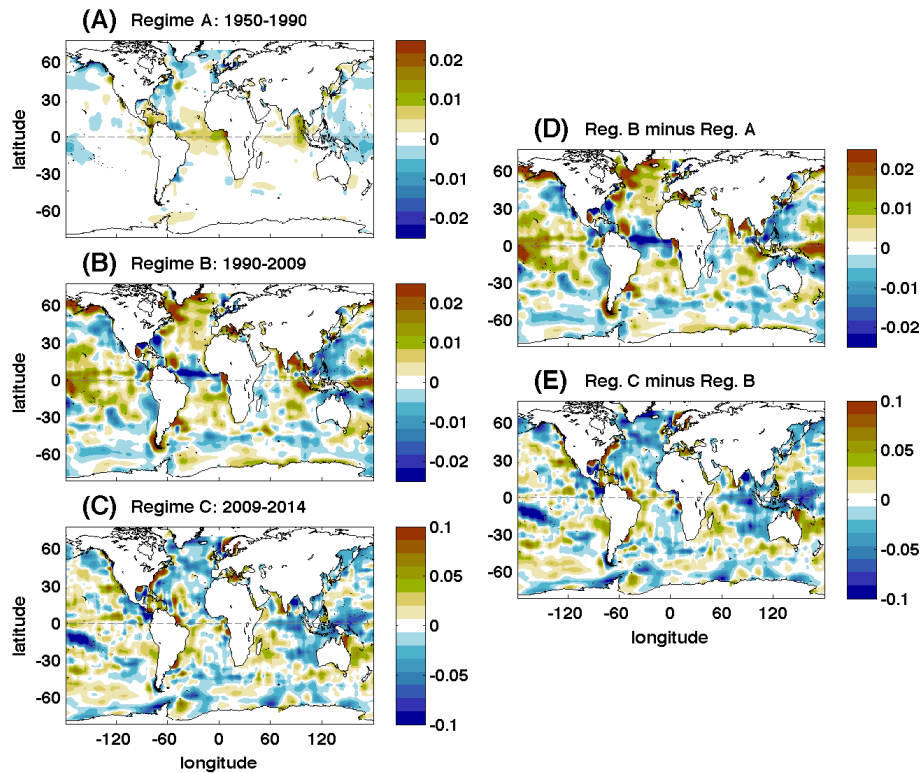


Figure 4. Surface salinity trend (yr^{-1}) for the three regimes estimated by the EM procedure using EN4 1950–2014 data: **(a)** Regime A: 1950–1990, **(b)** Regime B: 1990–2009; and **(c)** Regime C: 2009–2014. The right panels include the differences between the trends of **(d)** Regime B and A; and **(e)** Regime C and B. Note the different (four times larger) color scale for panels **(c)** and **(e)**.

Changes in surface salinity trend

A. L. Aretxabaleta et al.

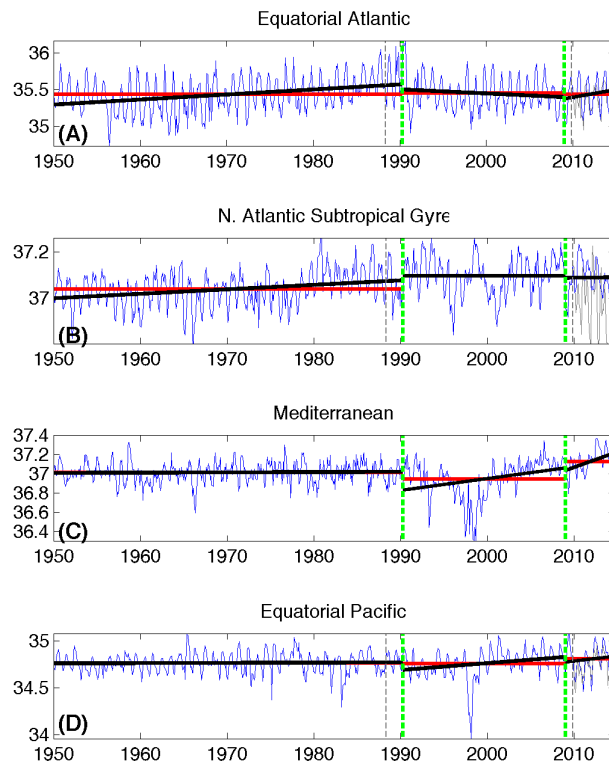


Figure 5. Average surface salinity time series (blue) for four example regions: **(a)** Equatorial Atlantic (5° S– 5° N), **(b)** North Atlantic Subtropical Gyre (15° – 30° N), **(c)** Mediterranean; and **(d)** Equatorial Pacific (5° S– 5° N). The green dashed lines indicate the separation (breakpoint) between regimes. The red lines are the average salinity for each regime and the black lines represent the trends for each regime. The gray lines for the period 2010–2014 correspond with the SMOS data average for each region (not Mediterranean). Note the change in the salinity range (vertical scale) in each panel.

[Title Page](#)[Abstract](#)[Introduction](#)[Conclusions](#)[References](#)[Tables](#)[Figures](#)[Back](#)[Close](#)[Full Screen / Esc](#)[Printer-friendly Version](#)[Interactive Discussion](#)

Changes in surface salinity trend

A. L. Aretxabaleta et al.

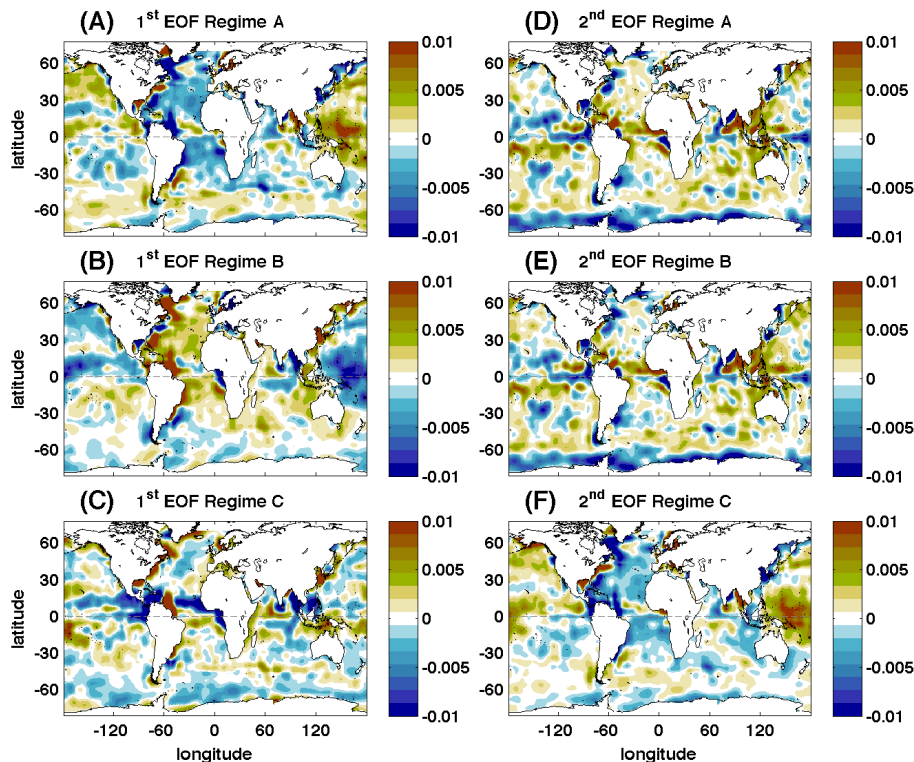


Figure 6. Main modes of variability of the EN4 1950–2014 salinity. First (a) and second (d) modes for Regime A (1950–1990). First (b) and second (e) modes for Regime B (1990–2009). First (c) and second (f) modes for Regime C (2009–2014).

Title Page

Abstract

Introduction

Conclusions

References

Tables

Figures

◀

▶

◀

▶

Back

Close

Full Screen / Esc

Printer-friendly Version

Interactive Discussion



Changes in surface salinity trend

A. L. Aretxabaleta et al.

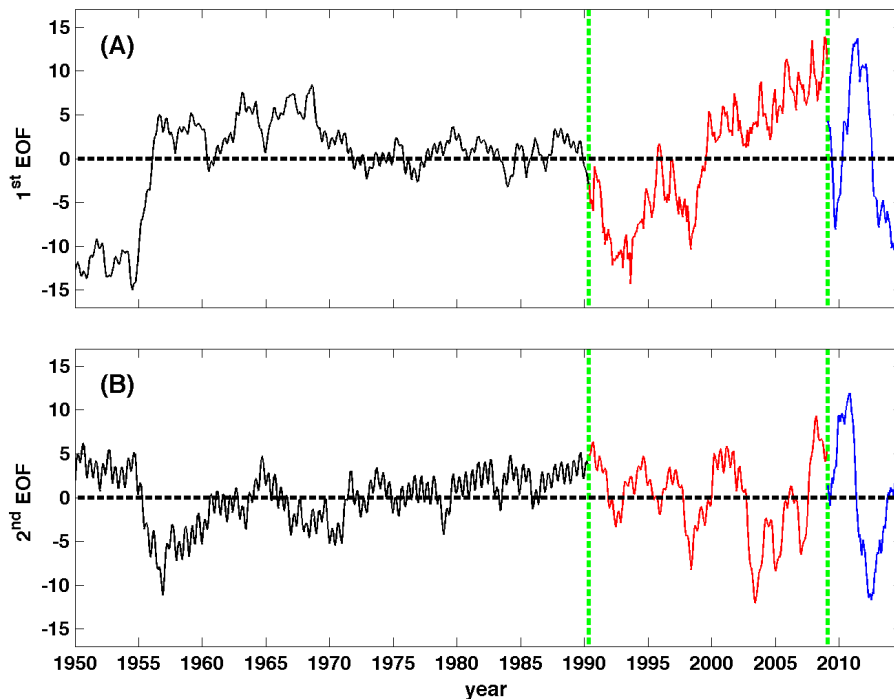


Figure 7. Time series of modes of variability of the EN4 1950–2014 salinity. First (a) and second (b) modes for Regime A (1950–1990), B (1990–2009) and C (2009–2014). The green dashed lines indicate the separation (breakpoint) between regimes.

Title Page

Abstract

Introduction

Conclusions

References

Tables

Figures

◀

▶

◀

▶

Back

Close

Full Screen / Esc

Printer-friendly Version

Interactive Discussion



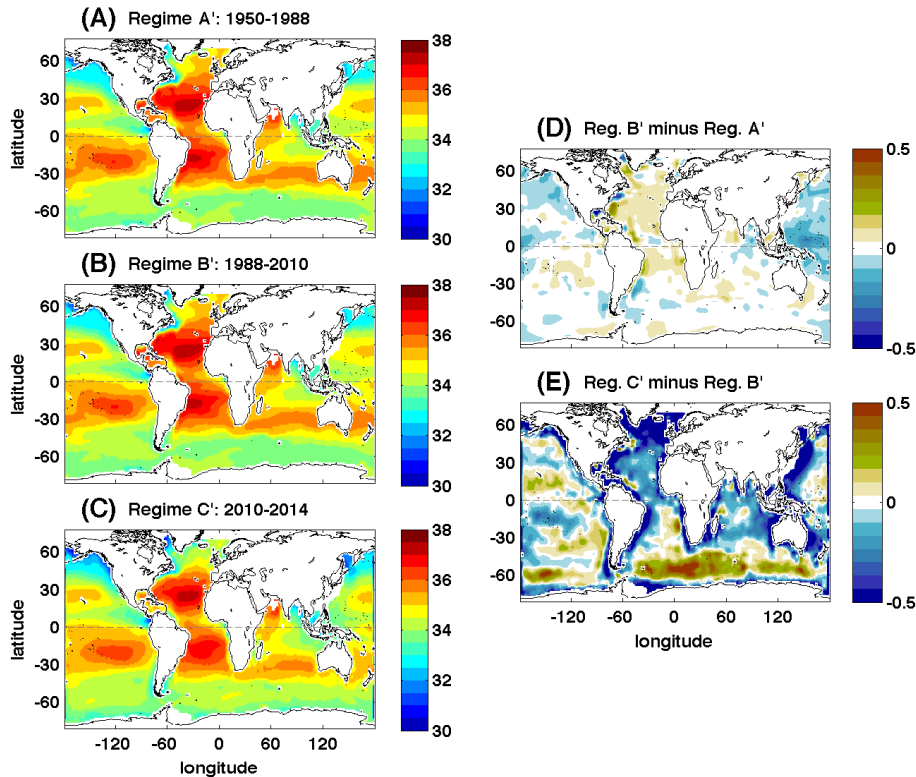


Figure 8. Mean surface salinity for the three regimes estimated by the EM procedure using combined EN4 and SMOS data: **(a)** Regime A': 1950–1988, **(b)** Regime B': 1988–2010; and **(c)** Regime C': 2010–2014. The differences between the means of Regime B' and A' **(d)** and Regime C' and B' **(e)** are also included.

Changes in surface salinity trend

A. L. Aretxabaleta et al.

Title Page

Abstract Introduction

Conclusions References

Tables Figures

◀ ▶

◀ ▶

Back Close

Full Screen / Esc

Printer-friendly Version

Interactive Discussion



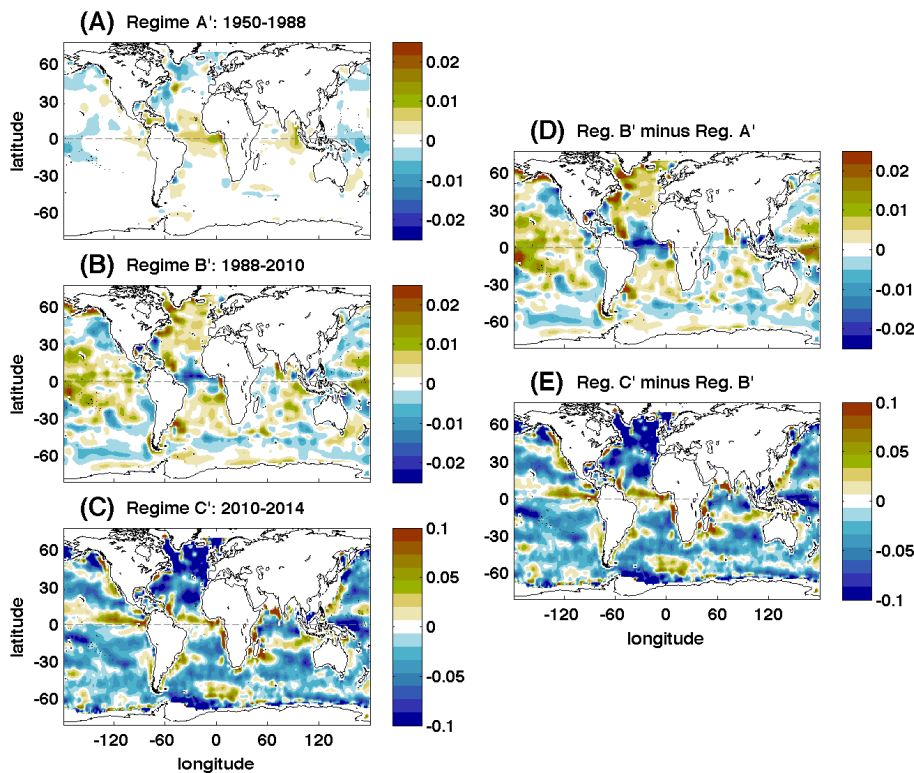


Figure 9. Surface salinity trend for the three regimes estimated by the EM procedure using combined EN4 and SMOS data: **(a)** Regime A': 1950–1988, **(b)** Regime B': 1988–2010; and **(c)** Regime C': 2010–2014. The differences between the trends of Regime B' and A' **(d)** and Regime C' and B' **(e)** are also included. Note the different (four times larger) color scale for panels **(c)** and **(e)**.

Changes in surface salinity trend

A. L. Aretxabaleta et al.

Title Page

Abstract

Introduction

Conclusions

References

Tables

Figures

◀

▶

◀

▶

Back

Close

Full Screen / Esc

Printer-friendly Version

Interactive Discussion

